ELECTRONIC SUPPLEMENTARY INFORMATION:

Unraveling the contributions to the spectral shape of flexible dyes in solution: insights on the absorption spectrum of an oxyluciferin analogue.

Javier Cerezo,[*a,b] Cristina García-Iriepa,[*c,d] Fabrizio Santoro,[b] Isabelle Navizet,[e] and Giacomo Prampolini[*b]

Contents

[a] *Departamento de Química and Institute for Advanced Research in Chemical Sciences (IAdChem), Universidad Autónoma de Madrid, 28049 Madrid, Spain. E-mail: javier.cerezo@uam.es*

[b] *CNR–Consiglio Nazionale delle Ricerche, Istituto di Chimica dei Composti Organo Metallici (ICCOM-CNR), SS di Pisa, Area della Ricerca, via G. Moruzzi 1, I-56124 Pisa, Italy. E-mail: giacomo.prampolini@pi.iccom.cnr.it*

[c] *Universidad de Alcalá, Departamento de Química Analítica, Química Física e Ingeniería Química, Grupo de Reactividad y Estructura Molecular (RESMOL), 28806 Alcalá de Henares (Madrid), Spain. E-mail: cristina.garciai@uah.es*

[d] *Universidad de Alcalá, Instituto de Investigación Química "Andrés M. del Río" (IQAR), 28806 Alcalá de Henares (Madrid), Spain*

[e] *Univ Gustave Eiffel, Univ Paris Est Creteil, CNRS, UMR 8208, MSME, F-77454 Marne-la-Vallée, France*

S1 LVC model

In cases where interstate couplings need to be considered in the calculation (see Section 4.2.1), we abandon the Born-Oppenheimer approximation. In this scenario, the vibronic absorption spectrum cannot be obtained taking the transition from the ground state to each excited state independently. We thus resort to a Linear Vibronic Coupling (LVC) model and propagate using Quantum Dynamics (QD) the wavepacket corresponding to the vibrational ground state in each excited electronic state. The initial wavepacket corresponds to the lowest vibrational states in the ground electronic state, i.e., defined around the vertical or the Franck Condom geometry (reference geometry). The coupled excited potential energy surfaces (PESs) are described with LVC model, as quadratic (harmonic) diabatic states, $\{|d_i\rangle\}$, with coulings that linearly depend on nuclear coordinates. The resulting coupled Hamiltonian reads,

$$\hat{\mathscr{H}} = \sum_i \left(\hat{K} + V_{ii}^{dia}(\mathbf{q}) \right) |d_i\rangle\langle d_i| + \sum_{i,j>i} V_{ij}^{dia}(\mathbf{q}) \left(|d_i\rangle\langle d_j| + |d_j\rangle\langle d_i| \right) \tag{S1}$$

where $\hat{K}$ is the kinetic energy operator, V_{ii}^{dia} refers to the potential energy of the i-th diabatic state and V_{ij}^{dia} is the potential coupling between i-th and j-th diabatic states. We adopt dimensionless normal coordinates evaluated at the ground state, $\mathbf{q}$, and conjugated momenta, $\mathbf{p}$, to express the different terms:

$$\hat{K} = \mathbf{p}^t \Omega \mathbf{p} \tag{S2a}$$

$$V_{ii}^{dia}(\mathbf{q}) = E_i^0 + \lambda_{ii}^t \mathbf{q} + \frac{1}{2}\mathbf{p}^t \Omega \mathbf{p} \tag{S2b}$$

$$V_{ij}^{dia}(\mathbf{q}) = \lambda_{ij}^t \mathbf{q} \tag{S2c}$$

where Ω is a diagonal matrix containing the ground state frequencies. Harmonic diabatic potentials are expanded at ground state minimum using ground state Hessian, with constant term E_i^0 (diabatic vertical energy) and linear term λ_{ii} (diabatic gradient). The potential coupling, V_{ij} is expanded linearly assuming no coupling at the reference geometry and with a linear term λ_{ij}. Note that when the couplings are neglected, the LVC model leads to the VG model.

The diabatic states are defined to as the adiabatic states at the reference geometry (ground state minimum), i.e., the potential coupling is zero at that geometry. The linear term, λ_{ij}, is then obtained by numerical differentiation, carrying out a diabatization at each displaced geometry. The diabatization procedure provides the rotation, $\mathbf{D}$, of the adiabatic states at the displaced geometry, Δ_α, that yields the maximum overlap between the rotated (diabatic) states and the reference states. Namely, if we take the diabatic basis, $|\mathbf{d}\rangle = (|d_1\rangle, |d_2\rangle \ldots)^t$, and adiabatic one, $|\mathbf{a}\rangle = (|a_1\rangle, |a_2\rangle \ldots)^t$, they are related through,

$$|\mathbf{d}\rangle = \mathbf{D}(\Delta_\alpha)|\mathbf{a}(\Delta_\alpha)\rangle \tag{S3}$$

where we have made explicit the dependence of the rotation and the adiabatic states with the displacement. The rotation can be computed from the overlap between the adiabatic states at the reference ($\Delta_\alpha = 0$) and displaced geometries, $\mathbf{S} = \langle \mathbf{a}(0)|\mathbf{a}(\Delta_\alpha)\rangle$, as $\mathbf{D} = (\mathbf{S}^t\mathbf{S})^{-1/2}\mathbf{S}^1$. The diabatic potential is computed from the diagonal adiabatic one applying this rotation,

$$\mathbf{V}^{dia}(\Delta_\alpha) = \mathbf{D}^t(\Delta_\alpha)\mathbf{V}^{adia}(\Delta_\alpha)\mathbf{D}(\Delta_\alpha) \tag{S4}$$

which are used to carry out the numerical differentiation.

Further adopting the FC approximation to describe the transition dipoles from the ground state to each (diabatic) state, μ_{gi}^0, the non-adiabatic electronic spectrum, at $0\,\mathrm{K}$, can be computed from the propagation of the initial wavepacket (ground vibrational wavefunction at the ground electronic state), $|\mathbf{0}\rangle$, over all diabatic states, $|d_i\rangle$, as [2]

$$\varepsilon(\omega) = \frac{2\pi\omega N_A}{3 \times 1000 \times \ln 10 \times \hbar \times (4\pi\varepsilon_0)} \int_{-\infty}^{\infty} dt e^{i\omega_0 t} e^{i\omega t} \sum_{i,j} (\mu_{gj}^0)^t \mu_{gi}^0 \langle \mathbf{0}; d_j | e^{-it\hat{\mathscr{H}}/\hbar} | d_i; \mathbf{0} \rangle$$

$$= \sum_i \varepsilon_{ii}(\omega) + \sum_{i,j \neq i} \varepsilon_{ij}(\omega) \tag{S5}$$

where $\hbar\omega_0$ is the zero point energy at the ground electronic state and $|d_i; \mathbf{0}\rangle = |d_i\rangle|\mathbf{0}\rangle$. We have make explicit that the expression contains both auto-correlation functions, $\varepsilon^{auto} = \varepsilon_{ii}(\omega)$, and cross-correlation functions, $\varepsilon^{cross} = \varepsilon_{ij}(\omega)$.

S2 QMD-FF parameterization

S2.1 General background

The Quantum Mechanically Derived Force Field (QMD-FF) employed in this work has been parameterized specifically for 5,5-CprOxyLH. In the following a brief description of the parameterization procedure will be given, although all the details can be found in the original papers[3,4]. The QMD-FF for a system composed by a flexible dye (5,5-CprOxyLH) solvated by N_{solv} solvent molecules (H_2O) may be partitioned in an intra-molecular term E_{QMD-FF}^{intra} and an inter-molecular one, E_{QMD-FF}^{inter}:

$$E_{QMD-FF}^{tot} = E_{QMD-FF}^{intra} + E_{QMD-FF}^{inter} \tag{S6}$$

When a rigid FF is adopted for the solvent (as in the TIP3P H_2O model, *vide infra*) the E_{QMD-FF}^{intra} only acts on solute's flexibility, whereas E_{QMD-FF}^{inter} describes the solute's interaction with the solvent and the interactions among solvent molecules. The parameters defining the intra-molecular term have been obtained in this work with the JOYCE procedure,[3–5] i.e. by deriving them with respect to the reference QM data described in the main text. The 5,5-CprOxyLH specific QMD-FF thus takes the standard expression:

$$E_{QMD-FF}^{intra(\mathbf{r}^{ric}, \mathbf{R}^{ric})} = E_s(\mathbf{r}^{ric}) + E_b(\mathbf{r}^{ric}) + E_{st}(\mathbf{r}^{ric}) + E_{ft}(\mathbf{R}^{ric}) + E_{Nb}^{intra}(\mathbf{R}^{ric}) \tag{S7}$$

where the first three terms refer to the energy of stretching (E_s), of angle bending (E_b) and of stiff dihedral (E_{st}) which depend on stiff redundant internal coordinates (RICs, $\mathbf{r}^{ric}$). The last two terms, which refer to the energy of flexible dihedrals and intramolecular non-bonded terms, depend on more soft RICs ($\mathbf{R}^{ric}$), which are expected to present an enhanced flexibility.[6] Concretely, harmonic potentials are employed to approximate the former stiff terms:

$$E_s = \frac{1}{2} \sum_i^{N_{bonds}} k_i^s (r_i - r_i^0)^2 \; ; \; E_b = \frac{1}{2} \sum_i^{N_{angles}} k_i^b (\theta_i - \theta_i^0)^2 \; ; \; E_{st} = \frac{1}{2} \sum_i^{N_{dihedrals}} k_i^{st} (\phi_i - \phi_i^0)^2 \tag{S8}$$

while the softer terms are handled beyond harmonic approximation, and the large amplitude displacements induced by the rotation of flexible dihedral, are accounted either by Fourier-like expansions for flexible dihedrals or Lennard-Jones (LJ) potential for non-bonded intra-molecular terms:

$$E_{ft} = \sum_{\mu}^{N_{dihedrals}} \sum_j^{N_{cos\mu}} k_{j\mu}^{ft} \left[1 + cos(n_j^\mu \delta_\mu - \gamma_j^\mu) \right] \tag{S9}$$

where δ_μ is the μ-th slow torsion, $k_{j\mu}^{ft}$ the force constant for the contribution with multiplicity n_j^μ and γ_j^μ a proper phase for that multiplicity, and

$$E_{Nb}^{intra} = \sum_i \sum_{i<j} 4\varepsilon_{ij}^{intra} \left[\left(\frac{\sigma_{ij}^{intra}}{r_{ij}} \right)^{12} - \left(\frac{\sigma_{ij}^{intra}}{r_{ij}} \right)^6 \right] + \left(\frac{q_i^{intra} q_j^{intra}}{(4\pi\varepsilon_0) r_{ij}} \right) \tag{S10}$$

where ε_{ij}^{intra} and σ_{ij}^{intra} as well as q_i^{intra} are tuned for specific pairs according to the standard JOYCE procedure.[3,5] It might be here worth mentioning that while in most popular transferable FFs the non-bonded contributions are automatically included among all possible pairs of interacting sites i-j adopting the same set of LJ and charge parameters for both inter-molecular and intra-molecular interactions. According to the JOYCE protocol,[3] intra-molecular LJ parameters may be different from the ones adopted for the description of inter-molecular interactions (see equation S12) and they can be

included in the QMD-FF just for selected intra-molecular atom pairs, thus allowing for a more specific parameterization.

The last term of equation (S6), E_{QMD-FF}^{inter}, accounts for the interactions between the solute and the solvent and among the solvent molecules, *i.e.*

$$E_{QMD-FF}^{inter} = \sum_{i=1}^{N_{solu}} \sum_{j=1}^{N_{solv}} E_{ij}^{solu-solv} + \sum_{i=1}^{N_{solv}} \sum_{j=1}^{N_{solv}} E_{ij}^{solv-solv} \tag{S11}$$

where E_{ij}^{x-solv} ($x = solu, solv$) takes the standard expression

$$E_{ij}^{x-solv} = \left(4\varepsilon_{ij}^{x-solv} \left[\left(\frac{\sigma_{ij}^{x-solv}}{r_{ij}} \right)^{12} - \left(\frac{\sigma_{ij}^{x-solv}}{r_{ij}} \right)^{6} \right] \right) + \left(\frac{q_i^x q_j^{solv}}{(4\pi\varepsilon_0) r_{ij}} \right) \tag{S12}$$

The first term in square brackets on the right side of equation (S12) is the standard 12-6 LJ potential, while the second term accounts for the Coulomb charge-charge interactions between the solute and the solvent or among the solvent molecules. The intermolecular LJ parameters adopted with the Joyce intramolecular FF are included in Table S1.

S2.2   5,5-CprOxyLH parameterization details

Both intra- and inter-molecular terms were specifically parameterized for the 5,5-CprOxyLH target molecule according to the procedure outlined in following:

- The choice of the 5,5-CprOxyLH atom types was aimed at finding the best compromise between FF specificity and a too redundant description. For this reason, all atoms were assigned to different atom-types, unless equivalent for symmetry, as shown in panel a) of Figure S1.
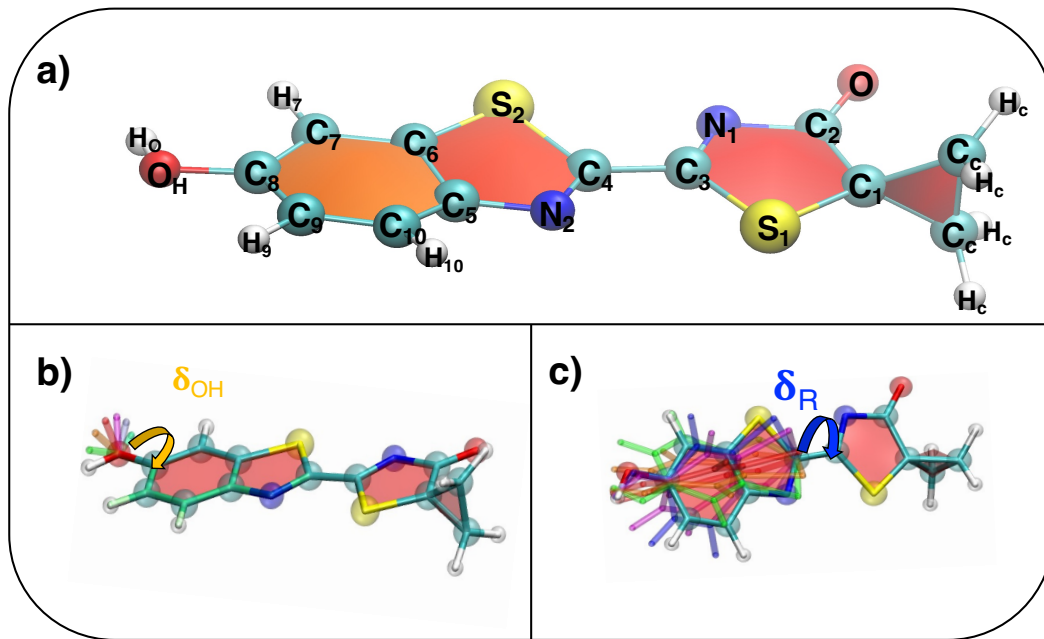
Fig. S1 QMD-FF parameterization settings: a) selected atom-types for the 5,5-CprOxyLH molecule; b-c) considered flexible dihedrals, δ_{OH} and δ_R, respectively.

- As far as the intra-molecular term, E_{QMD-FF}^{intra}, is concerned, all possible stretching and bending RICs coordinates were accounted for in the QMD-FF, together with all stiff dihedrals defined by quadruplets of atoms pertaining to the aromatic rings, also including "star-like" (or improper) dihedrals ruling the out-of-plane vibrations of the ring substituents and hydrogen atoms. Moreover, the flexible dihedrals, δ_{OH} and δ_R, shown in detail in panels b) and c) of Figure S1 were also considered in the RICs collection, while all intra-molecular nonbonded distances were excluded from the QMD-FF definition. A model potential function is then assigned to each RIC, depending on its stiffness as

discussed in Section S2.1.

- All intramolecular QMD-FF parameters were obtained with the JOYCE code,[7] by performing the usual two-step procedure: a first JOYCE cycle which fits all harmonic parameters at once and a second cycle, in which the harmonic parameters are fixed according to the Frozen Internal Rotation Approximation, and the parameters for the flexible dihedral are parameterized against the QM torsional relaxed energy scans. All parameters are reported in detail in the next section in Tables S2 to S5.

- Turning to the intermolecular term E_{QMD-FF}^{inter}, only the parameters concerning the solute-solvent interaction were refined specifically for the target system, whereas the solvent-solvent parameters were transferred from the TIP3P model.[8]. More specifically, the solute point charges q_i^{solu} entering in eq. (S12) were derived through the RESP procedure from the QM electronic density computed at the B3LYP/6-311G(2d,p) level on the isolated molecule in its optimized conformation, accounting for the (water) solvent by means of the C-PCM[9] method, as detailed in the main text. No further modification was instead accounted for the LJ terms, which were transferred from the OPLS FF.[10,11] All intermolecular parameters are reported in detail in Table S1.

S2.3 QMD-FF parameters

Atom type	σ	ε	q	Atom type	σ	ε	q
C_C	3.50	0.2761	-0.2290	C_6	3.55	0.2929	-0.0046
H_C	2.50	0.1255	0.1393	S_2	3.55	1.0460	-0.0282
C_1	3.50	0.2761	0.0516	C_7	3.55	0.2929	-0.1833
C_2	3.75	0.4393	0.6292	C_8	3.55	0.2929	0.1409
O	2.96	0.8786	-0.5031	C_9	3.55	0.2929	-0.1271
N_1	3.25	0.7113	-0.5108	C_{10}	3.55	0.2929	-0.2240
C_3	3.55	0.2929	0.1622	O_H	3.07	0.7113	-0.5188
S_1	3.55	1.0460	-0.0853	H_O	0.00	0.0000	0.4558
C_4	3.55	0.2929	0.2936	H_7	2.42	0.1255	0.2200
N_2	3.25	0.7113	-0.4424	H_9	2.42	0.1255	0.1457
C_5	3.55	0.2929	0.2558	H_{10}	2.42	0.1255	0.1734

Table S1 Inter-molecular 5,5-CprOxyLH parameters: σ (Å), ε (kJ/mol) and q (e$^-$) Atom types are shown in Figure S1. For the solvent (water), TIP3P parameters are used. For interactions between atoms of type i and j, the mixed σ_{ij} and ε_{ij} are obtained with the following geometric averages: $\sigma_{ij} = (\sigma_i \sigma_j)^{1/2}$ and $\varepsilon_{ij} = (\varepsilon_i \varepsilon_j)^{1/2}$

stretching	r^0	k^s	stretching	r^0	k^s
C_1-S_1	1.798	1888.76	S_1-C_3	1.771	1675.20
N_1-C_3	1.288	4606.62	N_1-C_2	1.406	2213.79
C_2-O	1.206	7071.03	C_2-C_1	1.512	1754.26
C_1-C_C	1.514	1776.95	C_C-C_C	1.492	2275.62
C_C-H_C	1.083	3308.93	C_3-C_4	1.451	2434.72
C_4-N_2	1.295	4669.48	N_2-C_5	1.371	3085.80
C_5-C_6	1.417	2061.74	C_6-S_2	1.743	2126.17
C_4-S_2	1.769	1530.87	C_5-C_{10}	1.400	3018.87
C_{10}-C_9	1.378	3560.00	C_9-C_8	1.409	2666.59
C_8-C_7	1.389	3156.27	C_7-C_6	1.389	3042.88
C_{10}-H_{10}	1.082	3348.42	C_9-H_9	1.085	3260.33
C_7-H_7	1.082	3353.11	C_8-O_H	1.361	3298.83
O_H-H_O	0.964	4917.44	C_1-C_8	8.564	270.63

Table S2 Intra-molecular 5,5-CprOxyLH stretching parameters: equilibrium distances r^0 are in Å and force constants k^s in kJ mol^{-1}Å^{-2}.

bending	θ^0	k^b	bending	θ^0	k^b
N_1-C_2-C_1	112.4	77.18	C_2-C_1-S_1	108.6	506.98
C_1-S_1-C_3	87.7	1107.22	N_1-C_3-S_1	119.4	842.15
C_2-N_1-C_3	112.0	784.07	N_1-C_2-O	124.6	662.22
O-C_2-C_1	123.0	406.86	C_2-C_1-C_C	118.1	84.82
C_C-C_1-S_1	122.9	411.01	C_1-C_C-H_C	117.2	321.55
H_C-C_C-C_C	118.0	249.26	H_C-C_C-H_C	116.0	160.99
N_1-C_3-C_4	122.2	74.76	S_1-C_3-C_4	118.5	74.76
C_3-C_4-N_2	123.7	421.71	C_4-N_2-C_5	111.1	249.60
C_5-C_6-S_2	109.5	891.84	C_4-S_2-C_6	88.1	872.48
N_2-C_4-S_2	116.2	974.34	C_3-C_4-S_2	120.1	205.40
N_2-C_5-C_6	115.2	607.67	N_2-C_5-C_{10}	125.4	706.53
C_5-C_{10}-C_9	119.2	651.49	C_{10}-C_5-C_6	119.4	272.88
C_{10}-C_9-C_8	120.8	633.08	C_9-C_8-C_7	121.2	323.01
C_8-C_7-C_6	117.8	690.29	C_5-C_6-C_7	121.7	265.29
C_7-C_6-S_2	128.9	692.27	C_5-C_{10}-H_{10}	119.4	268.41
H_{10}-C_{10}-C_9	121.4	349.87	C_{10}-C_9-H_9	120.1	372.47
H_9-C_9-C_8	119.2	272.63	C_8-C_7-H_7	119.5	317.65
H_7-C_7-C_6	122.7	282.01	C_9-C_8-O_H	121.7	764.88
O_H-C_8-C_7	117.1	642.05	C_8-O_H-H_O	109.5	448.22

Table S3 Intramolecular 5,5-CprOxyLH bending parameters: equilibrium angles θ^0 are in degree, force constants k^b in kJ mol^{-1}rad^{-2}.

dihedral	ϕ^0	k^{st}	dihedral	ϕ^0	k^{st}
N_1-C_2-C_1-S_1	0.0	125.98	C_2-C_1-S_1-C_3	0.0	125.98
C_1-S_1-C_3-N_1	0.0	125.98	C_2-N_1-C_3-S_1	0.0	125.98
C_3-N_1-C_2-C_1	0.0	125.98	O-C_2-C_1-C_C	-34.0	71.25
C_2-C_1-C_C-H_C	-1.8	125.95	H_C-C_C-C_C-H_C	0.0	24.21
C_4-N_2-C_5-C_6	0.0	147.00	N_2-C_5-C_6-S_2	0.0	147.00
C_5-C_6-S_2-C_4	0.0	147.00	N_2-C_4-S_2-C_6	0.0	147.00
S_2-C_4-N_2-C_5	0.0	147.00	C_5-C_{10}-C_9-C_8	0.0	79.36
C_6-C_5-C_{10}-C_9	0.0	79.36	C_{10}-C_5-C_6-C_7	0.0	79.36
C_8-C_7-C_6-C_5	0.0	79.36	C_{10}-C_9-C_8-C_7	0.0	79.36
C_9-C_8-C_7-C_6	0.0	79.36	O_H-C_8-C_7-H_7	0.0	79.36
H_9-C_9-C_8-O_H	0.0	79.36	H_{10}-C_{10}-C_9-H_9	0.0	79.36
C_1-S_1-C_3-C_4	180.0	142.98	C_2-N_1-C_3-C_4	180.0	142.98
C_2-S_1-C_4-C_1	0.0	142.98	C_3-C_4-N_2-C_5	180.0	70.02
C_3-C_4-S_2-C_6	180.0	70.02	C_4-N_2-C_5-C_{10}	180.0	32.87
C_7-C_6-S_2-C_4	180.0	32.87	C_{10}-C_9-C_8-O_H	180.0	79.36
O_H-C_8-S_2-C_6	180.0	79.36	C_2-N_1-O-C_1	0.0	71.25
C_4-N_1-S_1-C_3	0.0	142.98	C_4-C_3-N_2-S_2	0.0	70.02
C_8-C_7-C_6-S_2	180.0	32.87	N_2-C_5-C_{10}-C_9	180.0	32.87
C_9-C_5-H_{10}-C_{10}	0.0	79.36	C_8-C_{10}-H_9-C_9	0.0	79.36
C_6-C_8-H_7-C_7	0.0	79.36	C_7-C_9-O_H-C_8	0.0	79.36

Table S4 Intramolecular parameters for 5,5-CprOxyLH stiff harmonic torsions: equilibrium dihedral angles ϕ^0 are in degrees and force constants k^t in kJ mol^{-1} rad^{-2}.

dihedral	N_{cos}	n	k^{ft} (kJ/mol)	γ (degr)
N_1-C_3-C_4-N_2	7	0	8.480	0.00
		1	5.869	0.00
		2	-6.838	0.00
		3	0.997	0.00
		4	0.379	0.00
		5	0.186	0.00
		6	0.048	0.00
S_1-C_3-C_4-S_2	7	0	8.480	0.00
		1	5.869	0.00
		2	-6.838	0.00
		3	0.997	0.00
		4	0.379	0.00
		5	0.186	0.00
		6	0.048	0.00
C_9-C_8-O_H-H_O	7	0	4.240	0.00
		1	-0.180	0.00
		2	-8.875	0.00
		3	0.494	0.00
		4	0.199	0.00
		5	0.003	0.00
		6	-0.017	0.00

Table S5 Intra-molecular parameters for 5,5-CprOxyLH flexible torsions δ_R (first two rows) and δ_{OH} (last row): number of cosines n, γ (degrees) and force constants k^d in kJ mol^{-1}. See panels b) and c) of Figure S1. See Eq. S9.

S3   MD simulations

All simulations were performed with the GROMACS code,[12] in the NVT and NPT ensembles for the gas and the condensed phase, respectively. For the isolated molecule, a 5 ns trajectory at 298 K was produced, storing dye's conformations every 50 ps. Conversely, the solvated system was equilibrated in the NPT ensemble for 5 ns, keeping temperature (298 K) and pressure (1 atm) constant t in the NPT ensemble through the Berendsen algorithm.[13] Thereafter, a 10 ns production run was carried out, keeping the same temperature and pressure constant through the velocity-rescale[14] and Parrinello-Rahman[15] schemes, which are capable to preserve the correct statistics in the NPT ensemble. In all runs, no bond length was constrained and the time step was set to 0.25 fs. A cut-off distance of 12 Å was employed for short-range interactions, and the standard correction for energy and virial applied to LJ potentials. Long range electrostatic was accounted for by the particle mesh Ewald scheme (PME). Temperature and pressure coupling constant τ_T and τ_P were set to 0.1 ps and 5 ps, respectively.
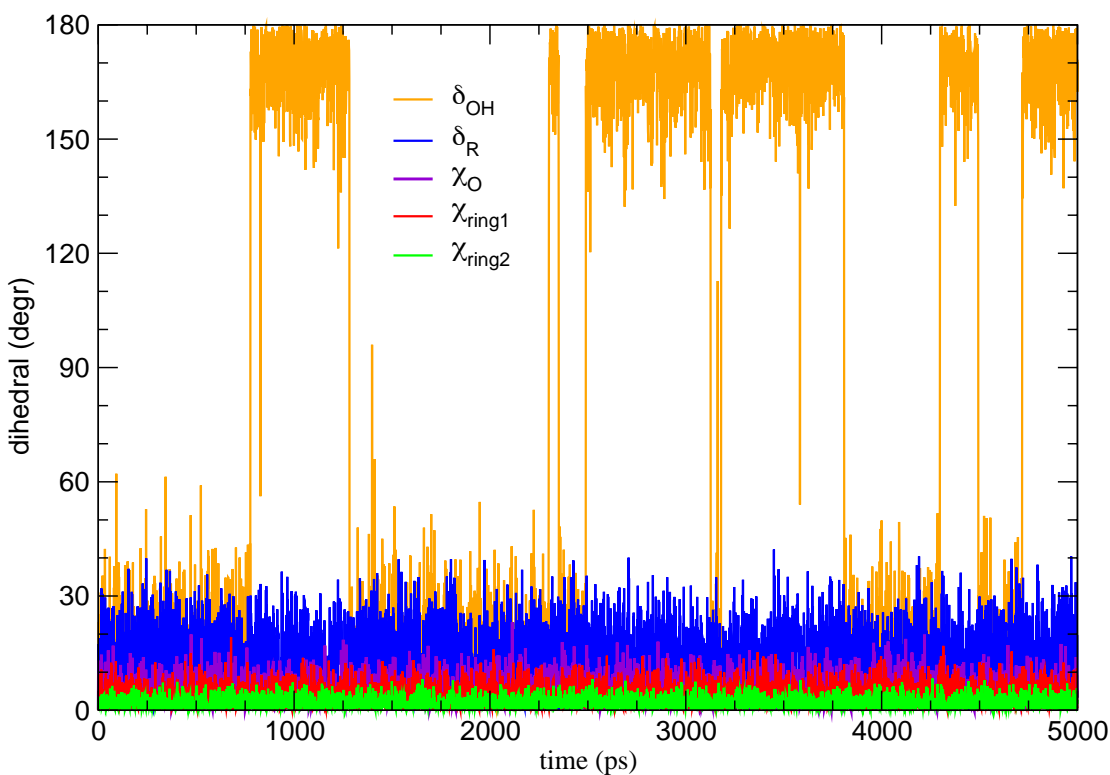
Fig. S2 Fluctuations of 5,5-CprOxyLH's flexible and stiff dihedral angles (see Figure 3 in the main text for definition) during the 5 ns gas phase runs at 298 K.

S4 TD calculations in the gas phase

Table S6 Description of the four lowest energy excited states of 5,5-CprOxyLH computed with B3LYP/6-311g(2d,p) in gas phase

Root	Sym	E_v (eV)	Osc. Str.	Exc. MO	character
1	A'	3.332	0.3069	H→L (86%)	$\pi\pi_1^*$
				H-1→L (12%)	
2	A''	3.461	0.0002	H-3→L (96%)	$n\pi_1^*$
3	A'	3.625	0.0998	H-1→L (72%)	$\pi\pi_2^*$
				H-2→L (17%)	
4	A'	3.713	0.2352	H-2→L (79%)	$\pi\pi_3^*$
				H-1→L (13%)	

HOMO-3　　　　　HOMO-2　　　　　HOMO-1

HOMO　　　　　LUMO
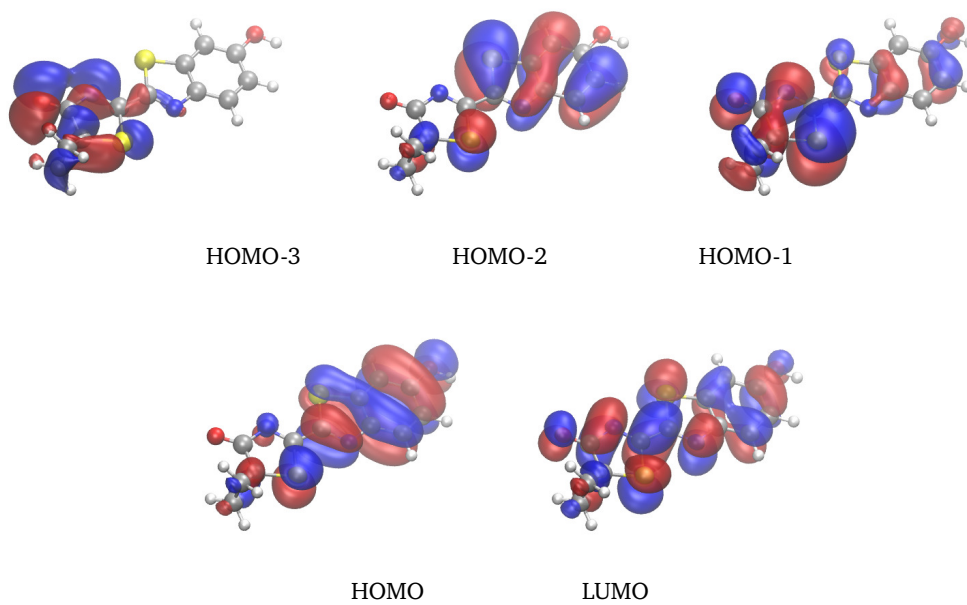
Fig. S3 Representation of the molecular orbitals involved in the electronic transitions S1-S4.
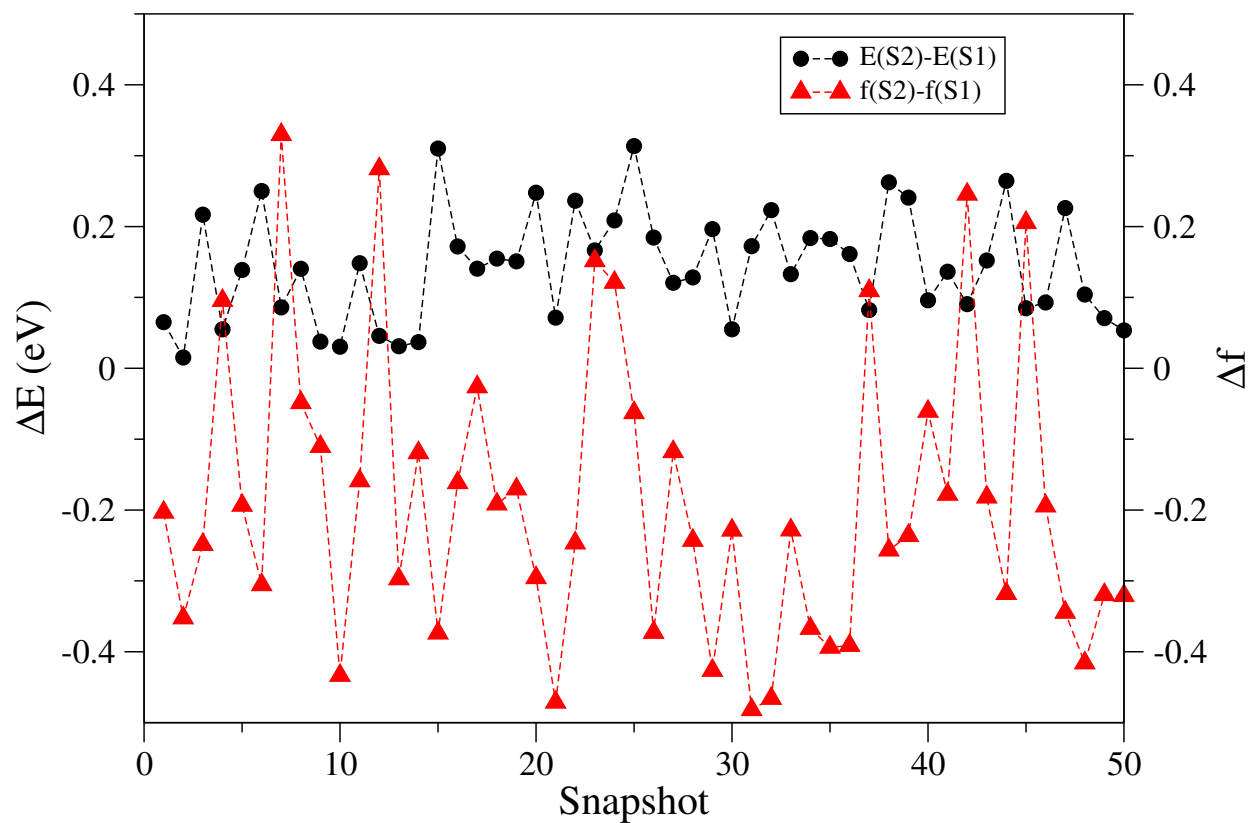
Fig. S4 Difference between the transition energies and oscillator strengths between states S1 and S2 along 50 snapshots extracted along an MD simulation of 5,5-CprOxyLH in gas phase.

S5 MD trajectories in water
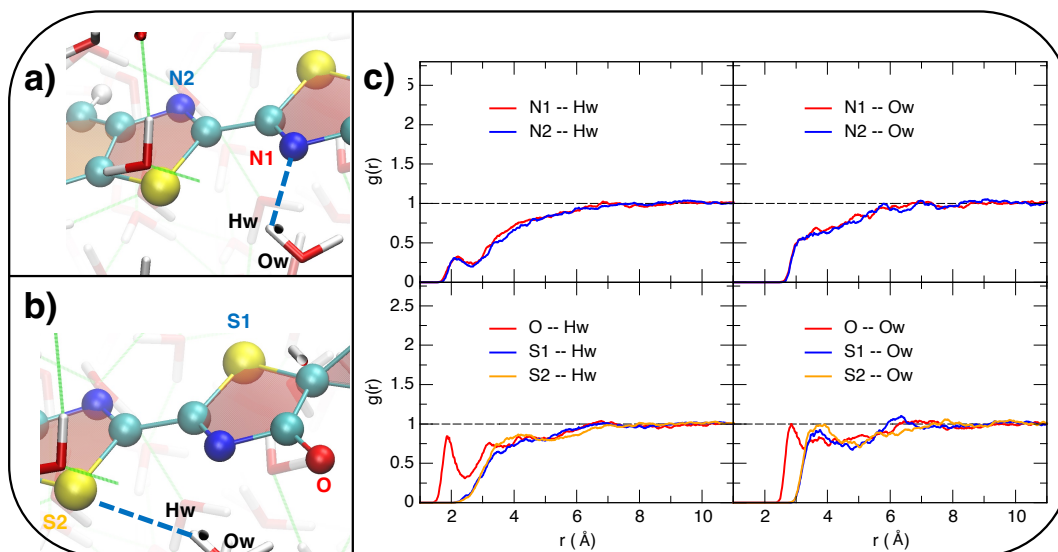
Fig. S5 Pair correlation functions between selected 5,5-CprOxyLH atom pairs (N1, S1, N2, S2 and O) and water atoms (Ow, Hw). a) Definition of N1 and N2 atoms located in each of the two rings; b) definition of sulfur atoms (S1 ans S2) and the keto oxygen atom (O); c) pair correlation functions, g(r) computed for nitrogen (top) and sulfur (bottom) atoms extracted from the MD trajectories. The g(r) functions concerning O are also reported for comparison.
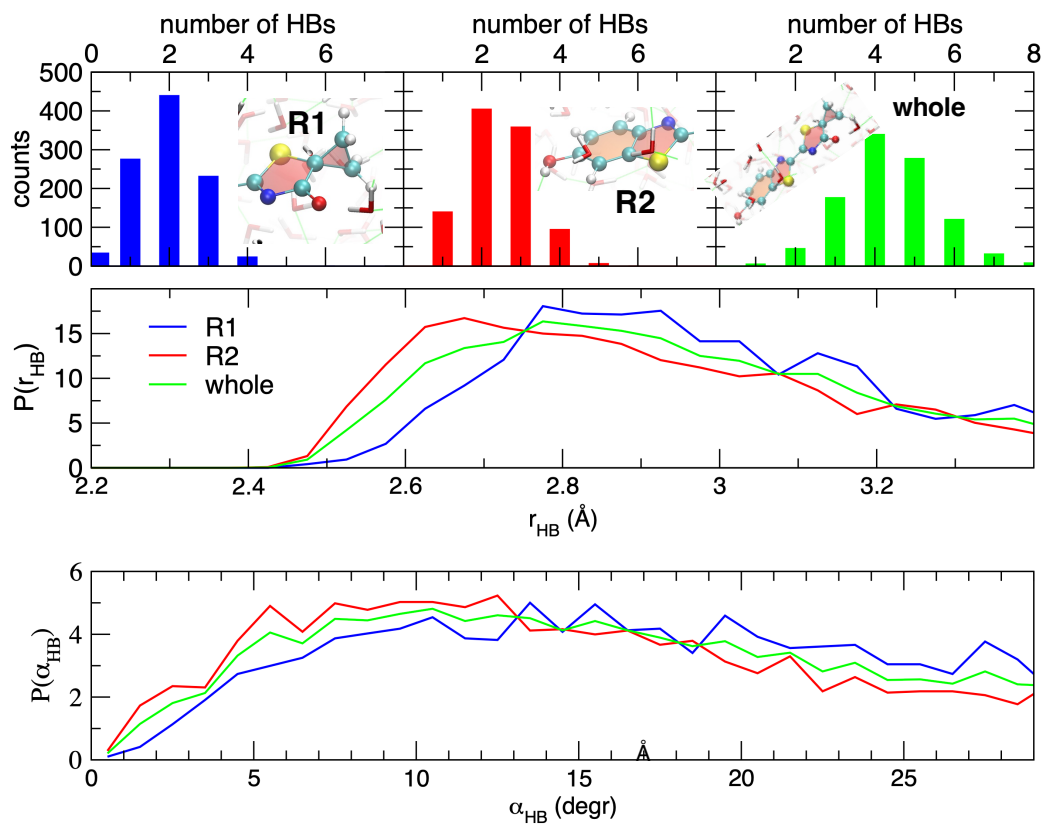
Fig. S6 Hydrogen bond (HB) analysis computed along the MD run in water. HB are identified for donor-acceptor pairs at a distance shorter than 3.5 Å and and angle hydrogen-donor-acceptor below 30°. Top panel: distribution of the number of HB established by 5,5-CprOxyLH with the surrounding water molecules. Middle panel: distribution of the HB distance r_{HB}. Bottom panel: distribution of the HB angle α_{HB}. All distributions are calculated for the five membered ring (R1, blue), the hydroxyl bearing ring (R2, red) and the whole chromophore (green).
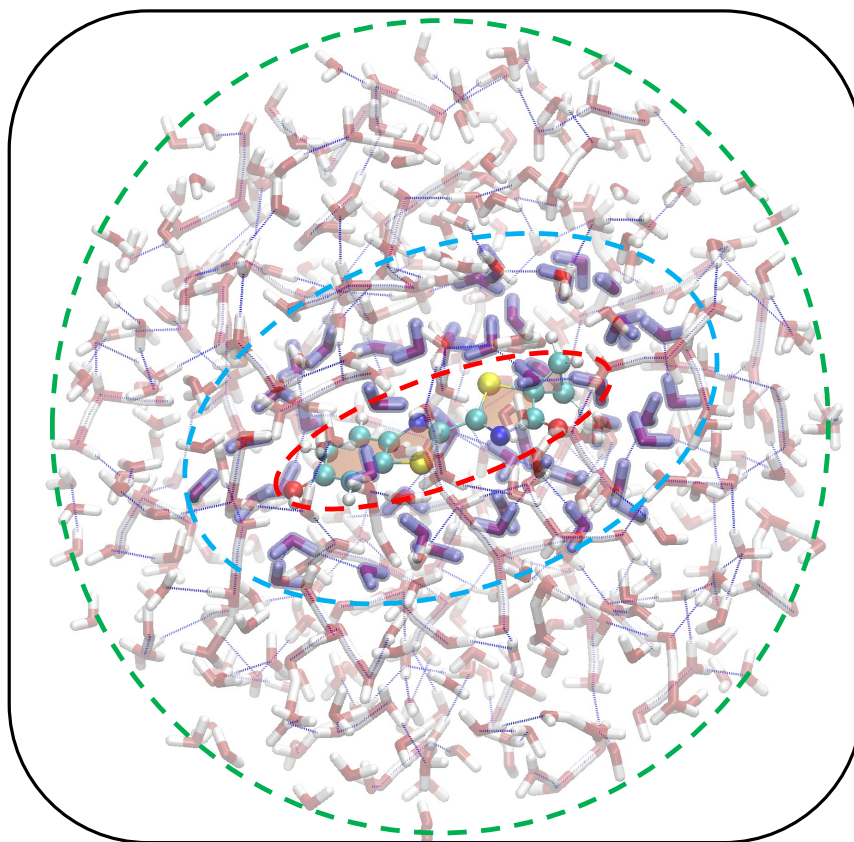
Fig. S7 QM/MM scheme with electrostatic embedding (EE) with point charges adopted for each snapshot extracted from the MD trajectories in solvent. QM level (red dashed line): solute 5,5-CprOxyLH (balls and stick representation); MM level (cyan dashed line): water molecules (liquorice, blue highlegthed) within 4 Å from every solute's atom; EE (green dashed line): all water molecules (liquorice, shaded) within 15Å from the solute's center.

S5.1 Distribution along selected normal modes

Here, we report the distribution of displacements for selected normal modes of the structures corresponding to the snapshots extracted along the MD simulation in water (with Joyce and AbrFF, see main text for a description of each FF). The reference normal modes are computed in the gas phase at B3LYP/6-31G(d) defined in terms of curvilinear internal coordinates. The selected normal modes (4 and 10) correspond to those that lead to a larger linear coupling between $n\pi^*$ and $\pi\pi^*$ states. The results are shown in Figure S8.
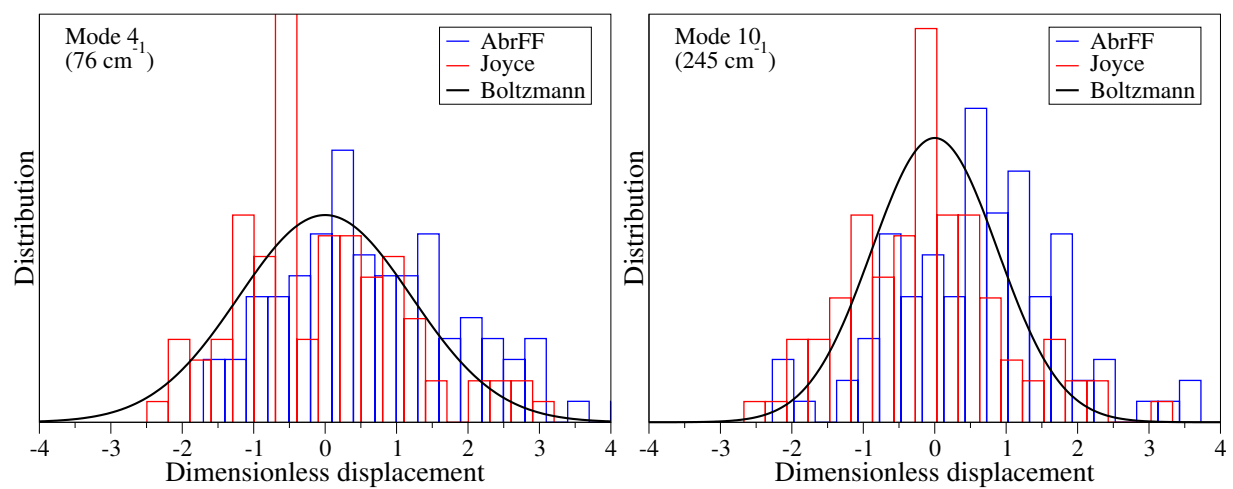
Fig. S8 Distribution of the dimensionless displacements along normal modes 4 and 10 (computed in gas phase) corresponding to structures extracted over the MD simulations in water using Joyce and AbrFF. The Boltmann distribution corresponding to the harmonic mode is included for reference.

S6 LVC calculation with PCM parameterization
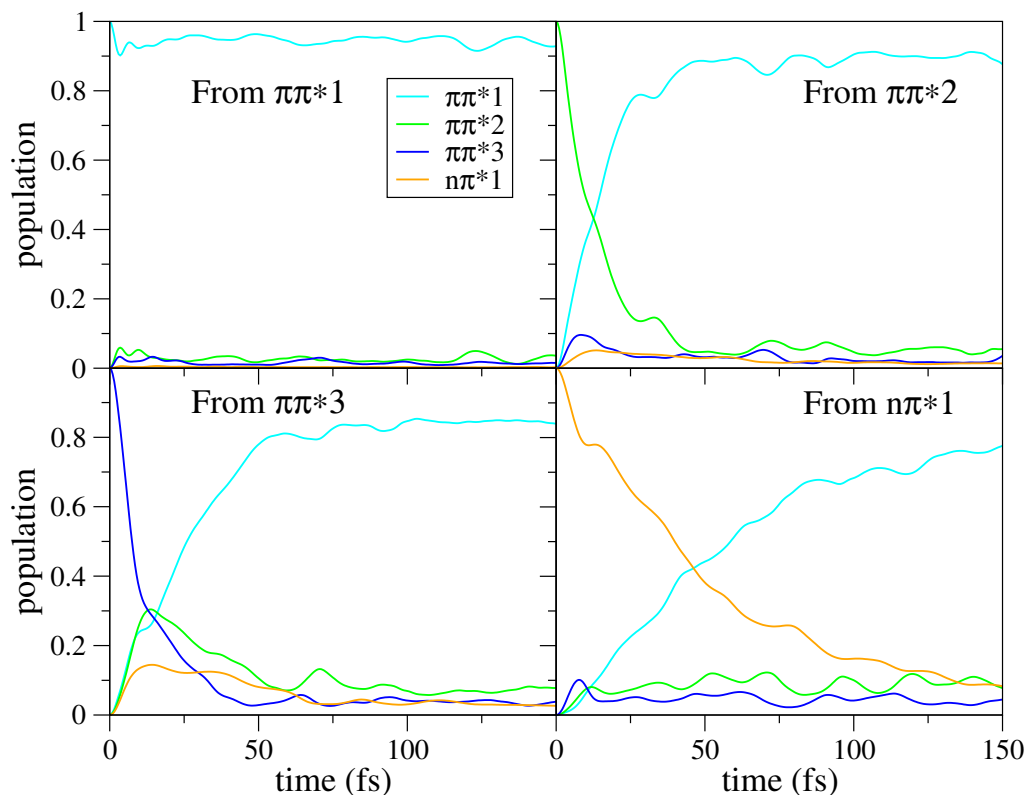
Fig. S9 Evolution of the electronic populations along QD propagation starting from the four different coupled diabatic excited states. LVC model parameterization is performed with B3LYP calculations in water accounter for through the PCM method. Although the color code is adopted, $\pi\pi^*2$ and $\pi\pi^*3$ are mixed with respect the same diabatic states in gas phase.
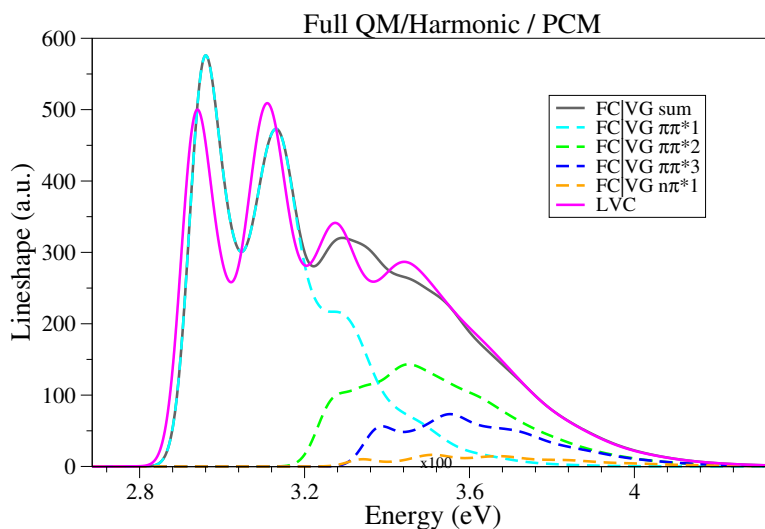
Fig. S10 Vibronic spectra of 5,5-CprOxyLH in the gas phase computed with fully QM methods on harmonic models. The spectrum, at T=0 K, is computed at nonadiabatic level with an LVC model, parameterized in water using the PCM method, including the four lowest state is compared with the spectra obtained switching off the couplings, i.e. at FC|VG level, and their sum. All spectra convoluted with a Gaussian with HWHM=0.04 eV

Notes and references

1 M. Yaghoubi Jouybari, Y. Liu, R. Improta and F. Santoro, *J. Chem. Theory Comput.*, 2020, **16**, 5792–5808.

2 Y. Liu, L. Martínez-Fernández, J. Cerezo, G. Prampolini, R. Improta and F. Santoro, *Chem. Phys.*, 2018, **515**, 452 – 463.

3 I. Cacelli and G. Prampolini, *J. Chem. Theory Comput.*, 2007, **3**, 1803–1817.

4 V. Barone, I. Cacelli, N. De Mitri, D. Licari, S. Monti and G. Prampolini, *Phys. Chem. Chem. Phys.*, 2013, **15**, 3736–3751.

5 J. Cerezo, G. Prampolini and I. Cacelli, *Theor. Chem. Acc.*, 2018, **137**, 80.

6 J. Cerezo, D. Aranda, F. J. Avila Ferrer, G. Prampolini and F. Santoro, *J. Chem. Theory Comput.*, 2020, **16**, 1215–1231.

7 I. Cacelli, J. Cerezo, N. De Mitri and G. Prampolini, JOYCE *2.10, a Fortran 77 code for intra-molecular force field parameterization. , available free of charge at http://www.iccom.cnr.it/en/joyce-2/, last consulted September 2022*.

8 W. L. Jorgensen, J. Chandrasekhar, J. D. Madura, R. W. Impey and M. L. Klein, *J. Chem. Phys.*, 1983, **79**, 926–935.

9 J. Tomasi, B. Mennucci and R. Cammi, *Chem. Rev.*, 2005, **105**, 2999–3094.

10 W. L. Jorgensen, D. S. Maxwell and J. Tirado-rives, *J. Am. Chem. Soc.*, 1996, **7863**, 11225–11236.

11 W. L. Jorgensen and J. Tirado-Rives, *Proc. Natl. Acad. Sci. USA*, 2005, **102**, 6665–70.

12 M. J. Abraham, T. Murtola, R. Schulz, S. Páll, J. C. Smith, B. Hess and E. Lindahl, *SoftwareX*, 2015, **1-2**, 19 – 25.

13 H. J. C. Berendsen, J. P. M. Postma, W. F. van Gunsteren, A. DiNola and J. R. Haak, *J. Chem. Phys.*, 1984, **81**, 3684–3690.

14 G. Bussi, D. Donadio and M. Parrinello, *J. Chem. Phys.*, 2007, **126**, 014101.

15 M. Parrinello and A. Rahman, *J. Appl. Phys.*, 1981, **52**, 7182–7190.